Interfacial dynamics of the rhomboidal pyramid pattern on ion-eroded Cu(110)

Alessandro Molle,* Francesco Buatier de Mongeot,† Anna Molinari, Corrado Boragno, and Ugo Valbusa
Dipartimento di Fisica, Università di Genova, Via Dodecaneso 33, I-16146 Genova, Italy
(Received 21 October 2005; published 17 April 2006)

Consecutive transitions between regular and periodic nanostructures induced by ion bombardment on the Cu(110) surface have been studied as a function of the sputtering parameters (primary ion energy, substrate temperature, and ion flux). The morphologies can vary from the well-known ripple patterns oriented along the two main symmetry directions of the fcc(110) substrate, to mounded structures, and include the far from equilibrium rhomboidal pyramid motif recently observed on the Rh(110) surface. The dependence of the nanostructure facet slope and lateral separation from ion energy allows us to identify a morphological regime accessed for low ion energy, below 500 eV, corresponding to the formation of rhomboidal pyramids. The dependence from the ion flux and substrate temperature bears strong similarities with a growth experiment, and is determined by the relaxation of isolated adatom and/or vacancy clusters created in the topmost surface layer by an ion impact. The selection of preferential step orientation and slopes follows from a delicate balance between the diffusion currents along the two main diffusion channels, the $\langle 1\bar{1}0\rangle$ and the $\langle 001\rangle$.

DOI: 10.1103/PhysRevB.73.155418 PACS number(s): 68.65.−k, 68.35.Fx, 68.47.De, 68.49.Jk

I. INTRODUCTION

According to a bottom-up approach, the achievement of a pattern formation of nanoscale sizes is often based on the self-organization of surface structures endowed with a controlled arrangement of steps and a prescribed periodicity. From this viewpoint, the ion erosion of monocrystalline metal substrates is well established as a tool to develop surface nanostructures, such as rippled corrugations or arrays of mounds[1–4] (for a review on the topics see Ref. 5). These patterns appear to be in close analogy with those obtained during epitaxial deposition[6] provided that the substrate temperature is properly rescaled. In fact, in spite of the conventional wisdom which pictures the sputtering process as a negative homoepitaxial deposition, i.e., a deposition of vacancies, single ion impact experiments on Ag(100) reveal that both adatom and vacancy clusters are produced under ion irradiation with the former clusters playing a primary role in the temperature dependence of the ion-induced kinetic roughening due to their higher mobility.[7] This aspect is further complicated in the presence of an anisotropic fcc(110) substrate where the diffusion paths are influenced by the rectangular symmetry of the surface unit cell thus following preferentially the $\langle 1\bar{1}0\rangle$ close-packed channels. Very recently we demonstrated that by tuning the concentration and the diffusivity of the surface defects during ion irradiation of fcc(110) metal surfaces one can observe consecutive transitions between rippled states, passing through intermediate states of mounds, which in turn can consist in rectangular mounds (RM) or, unexpectedly, in rhomboidal pyramids (RP), depending on the main parameters of the sputtering process (e.g., the impact energy, the substrate temperature during sputtering, and the ion flux).[1] Transitions between different morphological states are strictly related to the preferential selection of step edges with a lower advancement rate. The question whether during ion bombardment a particular step front prevails on the others depends on the thermal hierarchy of the interlayer and intralayer channels of kinetic mass transport. Surface destabilization by ion irradiation can be described by the phenomenological continuum approach which describes the global mobility of the surface defects in terms of a net current density.[1] Of course, a continuum theory only accounts for a coarse-grained description of the kinetic processes on a relatively large time scale and neglects the atomistic mechanisms of transport as well as the ion-surface collision transients. Nevertheless, in Ref. 1 a qualitative parallelism has been established between the morphological phase diagram of the continuum model of Refs. 8 and 9 and the experimental observations of a complete set of morphological states on the ion irradiation of the Rh(110) and Cu(110) substrates, using the substrate temperature T, the ion flux f, and the impact energy ε as parameters. According to this similarity, in steady-state conditions, i.e., for a saturated concentration of mobile species during irradiation, the diffusion of surface defects can be treated in a unified scheme both under the erosion as well as under the growth condition by considering a nonequilibrium, tilt-dependent flux of defects $\mathbf{J_{up}}(\mathbf{m}=\boldsymbol{\nabla} h)$ ($\mathbf{m}$ is the local slope vector and h is the surface profile) as responsible for the surface instability which gives rise to pattern formation. The destabilizing $\mathbf{J_{up}}$ term derives from the anisotropic diffusion uphill bias generated by the Ehrlich-Schwoebel (ES) barrier at the step edges of the (110) terraces. Kinetically induced structures are reached whenever steps rearrange by selecting local surface slopes $\mathbf{m}^*$ which minimize the $\mathbf{J_{up}}$ current, i.e., for stable zero solutions of $\mathbf{J_{up}}$.[10,11] Following the outline of Ref. 8, the arrangement of each morphological state depends on the vectorial character of the $\mathbf{m}^*$ solutions. In more detail, nonequivalent pairs of doubletlike solutions [$\mathbf{m}^*=(\pm m_1,0)$, or $(0,\pm m_2)$] identify two kinds of rippled structures, which are experimentally observed at low temperature (LTR state) and at high temperature (HTR states) depending on whether the faceting (and the periodicity) is extended along the $\langle 1\bar{1}0\rangle$ or the $\langle 001\rangle$ direction, respectively (a similar notation is employed in Ref. 12). The coexistence of both pairs of doubletlike solutions [$\mathbf{m}^*=(\pm m_1,0)$, and $(0,\pm m_2)$] expresses the oc-

currence of rectangularly faceted mounds with roof-top edges (RM pattern). Quartetlike solutions of the form $\mathbf{m}^* = (\pm m_1, \pm m_2)$ reflect the presence of two-dimensional pyramid structures having rhomboidal shaped step-edge lines (the novel RP state), shown in Ref. 1.

In Ref. 1 we have experimentally demonstrated the existence of the rhomboidal pyramid morphological state by diminishing the impact energy from 1000 eV down to 400 eV during the ion irradiation of Rh(110) and Cu(110) substrates held at the fixed substrate temperatures $T=450$ K and $T=230$ K, respectively. Motivated by these results, in this paper we extend our experimental observations of the fcc Cu(110) substrate by focusing more deeply on some peculiar aspects of the pattern formation such as the effect of the ion impact energy on the structural properties, the surface dynamics, and the thermal relaxation of the RP phase. The present experiments are wholly devoted to an *in situ* investigation on an ion bombarded fcc Cu(110) sample in a UHV condition (background pressure $\sim 10^{-10}$ mbar). The Cu(110) surface has been flattened by means of several sputtering and annealing cycles at about 800 K. To avoid relaxation of the surface pattern, after ion irradiation the substrate is rapidly cooled below 180 K. All sputtering experiments in this paper have been performed under close-to-normal ion beam incidence conditions (14.5° with respect to the surface normal) to avoid ion channeling. Measurements of consecutive transitions between morphological states are based on high resolution electron diffraction (SPA-LEED) inspections. This technique provides the great advantage to emphasize the facet distribution and the dominant Fourier modes intervening in the height-height correlation of the surface patterns via an incoherent sum of diffractive signals originated within regions over which the electron wave front is coherent (the instrumental transfer width amounts to ~ 0.1 μm). Information is thus integrated on a large scale "illuminated" portion of the surface corresponding to the beam diameter (approximately 0.1 mm). Another performance of the spot profile analysis concerns the determination of the average interfacial width W, whose scaling behavior is related to the nature of the kinetic processes intervening in the growth dynamics.[13,14] In fact, assuming the kinematical approximation to be valid, the decrease of the (0,0) peak intensity I_0, normalized by the total integrated intensity I_{tot} of the spot profile, near to the in-phase diffraction condition (integer values of the vertical scattering phase $S_z = k_z d/2\pi$, k_z, and d being the vertical momentum transfer and the monoatomic step height, respectively) is related to the average interface width W by the roughly Gaussian form.[15]

$$G_0(S_z) = I_0/I_{tot} \approx \exp\left[-2\frac{W^2}{d^2}(1-\cos 2\pi S_z)\right].$$

The presence of a lateral correlation Λ between the surface structures is perceived as an additional, phase independent, satellite splitting of the near to in-phase spot profile (i.e., for S_z close to integer values). According to this, Fig. 1 displays a three-dimensional plot of the (0,0) spot profile for a one-dimensional ripplelike pattern on the parallel momentum transfer plane $k_{\langle 001\rangle} - k_{\langle 1\bar{1}0\rangle}$ recorded at a scattering phase condition $S_z = 2.09$ such that two couples of satellites can be singled out (see also the grid lines in the contour plot of the spot profile reported in the inset). The inner couple of satellites derives from the average periodicity of the rippled corrugations whereas the outer couple, whose splitting turns out to be linearly dependent on the scattering phase, represents the diffraction from the slope selected ripple facets. The out-of-phase spot profiles, i.e., far from integer values of vertical scattering phase S_z, map the average facet slope of the surface structures and can thus be qualitatively compared with the theoretical $\mathbf{m}^*$ solutions of the $\mathbf{J_{up}}$ current. According to this, we have selected in Fig. 2 a sequence of out-of-phase diffraction maps ($S_z = 1.88$), acquired after an irradiation dose of 45 ML with an Xe^+ ion beam (1 ML nominally corresponding to 1.1×10^{15} ions/cm^2) at the fixed temperature $T=230$ K and ion flux $f=1$ ML/min, using the impact energy ε as a parameter. Then it is straightforward to attribute the twofold satellite splitting in the $\langle 1\bar{1}0\rangle$ reciprocal direction, observed after ion erosion at $\varepsilon=600$ eV [see Fig. 2(a)], to a doublet-type solution corresponding to the LTR state. This morphology is characterized by a one-dimensional rippled modulation of the surface profile with a spatial periodicity along $\langle 1\bar{1}0\rangle$ and a majority step elongated in the $\langle 001\rangle$ direction.[25] Following the same reasoning, the fourfold splitting of the diffraction profile in Fig. 2(c), obtained after erosion at $\varepsilon=400$ eV, corresponds to the quartet-type solution and, hence, to a RP pattern. Under the above condition of flux, there we interpret the RP diffraction pattern in terms of faceted mounds, with an arrangement of steps running along energetically unfavorable $\langle 1\bar{1}2\rangle$ directions of low symmetry, in agreement with the RP geometry observed on the Rh(110) surface[1] and theoretically predicted in Ref. 8. The spot profile recorded for the ion irradiation at $\varepsilon=500$ eV accounts for the morphological transition from the LTR to the RP faceting

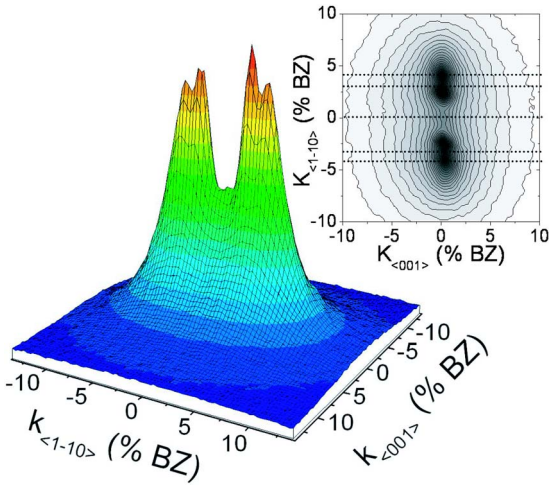

FIG. 1. (Color online) Three-dimensional plot of the (0,0) diffraction peak acquired under near-in phase conditions ($S_z=2.09$) by means of SPA-LEED for a rippled surface. The multiple satellite splitting indicates the presence of a well-defined lateral correlation and facets (see text for details). Inset: a two-dimensional contour plot of the spot profile (the dotted lines indicate the position of the two couples of satellites).

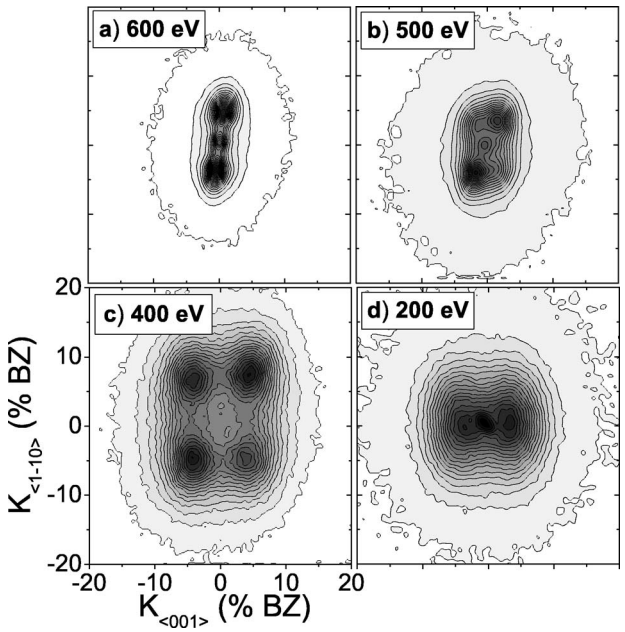

FIG. 2. Sequence of the out-of-phase SPA-LEED profile (S_z =1.88) after Xe^+ ion bombardment of a Cu(110) substrate at the temperature T=230 K, ion flux $f \approx 1$ ML/min, and total fluence $\Psi \approx 45$ ML, using the primary energy ε as a parameter: (a) ε =600 eV, (b) ε=500 eV, (c) ε=400 eV, and (d) ε=200 eV.

2showing a sort of a hybrid shape with an incipient splitting of the satellites along ⟨001⟩. The decrease of the impact energy down to 200 eV allows us to access once again a twofold splitting of the spot profile [see Fig. 2(d)], which, however, is 90° rotated with respect to the LTR one in Fig. 1(a). This indicates a further, consecutive transition towards the HTR state which was previously identified by scanning tunneling microscopy (STM).[25]

The quantitative analysis of the interfacial morphologies in Fig. 2 introduces a deeper discussion on the role of the impact energy upon the ion erosion of the Cu(110) surface, which will be developed in Sec. II by studying the energy dependence of relevant parameters of the surface nanostructures such as the correlation length Λ and the facet slope α. After elucidating the phenomenology of the LTR↔RP↔HTR transition in Sec. II and in Sec. III we investigate the surface evolution in the low energy regime of the RP state then comparing experimental evidences on the RP dynamics with theoretical predictions of Refs. 7 and 9. In Sec. IV we elucidate the instability of the RP state basing on an annealing experiment. Finally, in Sec. V, we suggest a physical description of the peculiar kinetic constraints occurring in the RP formation.

II. THE ROLE OF THE IMPACT ENERGY IN THE PATTERN FORMATION

In this section the behavior of the characteristic facet slope α and the correlation length Λ of the surface patterns is investigated vs variation of the impact energy in the range 200 eV$<\varepsilon<$2500 eV. These quantities are deduced from the satellite separation in the diffraction spot profile through

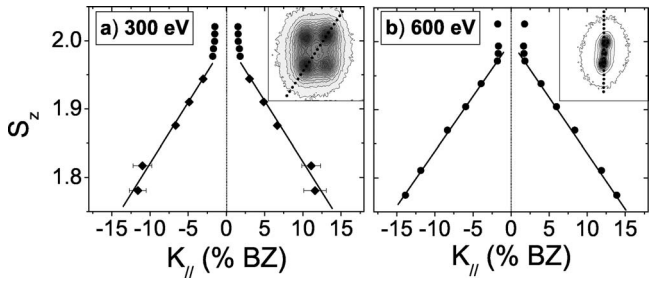

FIG. 3. Satellite separation vs the scattering phase for (a) the RP pattern obtained at ε=300 eV; (b) the LTR pattern obtained at ε =600 eV (the other parameters are set as in Fig. 2). The satellite splitting has been extracted along the reciprocal direction indicated within the spot profile in the insets by dotted lines except for the near-in-phase constant splitting, observed for the RP pattern and denoted by full circles in panel (a), which refers to linescans through the $\langle 1\bar{1}0 \rangle$.

the $\langle 1\bar{1}0 \rangle$ reciprocal direction as a function of S_z. For clarity we report in Fig. 3 two examples of such an analysis relating the RP and the LTR phases obtained after erosion at ε =300 eV [Fig. 3(a)] and ε=600 eV [Fig. 3(b)], respectively (the other parameters are the same as in Fig. 2). For both morphologies the periodicity occurs in the $\langle 1\bar{1}0 \rangle$ direction as demonstrated by the constant satellite separation near to the in-phase condition in both diagrams of Fig. 3. Conversely, the satellite peaks induced by faceting perceive the different orientation of the step arrangement in the surface patterns following diffraction rods along $\langle 1\bar{1}0 \rangle$ for the LTR state and along $\langle 1\bar{1}1 \rangle$ for the RP state. Note that the diffraction rods of the RP facets proceed along perpendicular directions with respect to the $\langle 1\bar{1}2 \rangle$ contour steps. Adopting a similar procedure, a complete set of data (Λ and α) is plotted in Fig. 4 as a function of the ion impact energy, ranging from 200 eV up to 2000 eV, for Xe^+ ion irradiation of the Cu(110) substrate at T=230 K.

The energy dependence of the correlation length Λ and of the average facet slope α immediately allows us to discrimi-

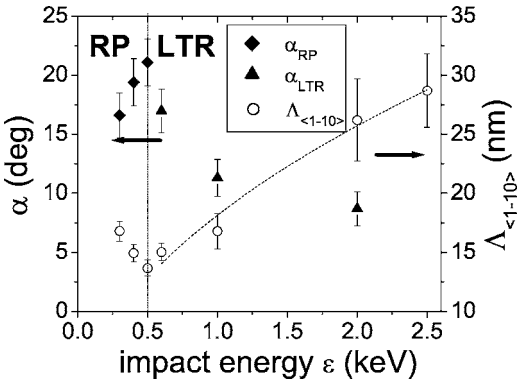

FIG. 4. Energy dependence of the correlation length Λ along the $\langle 1\bar{1}0 \rangle$ (open circles) and of the facet slope (rhomboidal points refer to RP facets, triangular point to LTR facets) of the surface structures obtained in the same conditions as Fig. 2. The vertical dotted line marks the border between the RP and the LTR regime (see text for details). The dashed line is a guide to the eye.

nate two opposite trends mutually intersecting in the point $\varepsilon^*=500$ eV. For 200 eV $<\varepsilon\leqslant 500$ eV, Λ is observed to follow a steep monotonic decrease with the energy, whereas, above 500 eV, this behavior is reverted in an increasing regime. An opposite trend is observed for the slope of the relevant surface structures: first increasing ($\varepsilon\leqslant 500$ eV) and then decreasing ($\varepsilon>500$ eV). The presence of two well-distinguished fashions for Λ and α reflects the occurrence of two structurally different morphological phases, the RP and the LTR, as already evidenced by the two-dimensional spot profiles in Fig. 2. In addition, a different faceting characterizes the two phases as reported by the energy dependence of the average facet slope in Fig. 4. The RP pattern develops facet slopes oriented along the $\langle 1\bar{1}1\rangle$ real space direction, having majority steps along the $\langle 1\bar{1}2\rangle$, as mentioned above, and following an almost linearly increasing behavior with the energy. On the other hand, the LTR morphology, in agreement with previous STM observations,[25] essentially consists in one-dimensional corrugations elongated in the $\langle 001\rangle$ direction with roof-top facets through the perpendicular $\langle 1\bar{1}0\rangle$ direction whose slopes are observed to relax with increasing energy.

A large variety of experimental results, not only in the case of metal surfaces, shows the increasing trend of the correlation length Λ vs the energy ε.[16] Restricting the consideration to single crystal metal surfaces, it is worthwhile to mention the linear behavior experienced by the correlation length of periodic and self-affine grooves induced on the Cu(001) surface via grazing incidence Ar^+ ion bombardment.[17] That result was explained in terms of irradiation-assisted diffusion where, during the finite time of the collision transient, a locally high density of supersaturated defects (adatoms, vacancies, clusters) can diffuse and form stable nuclei whose separation is proportional to the transferred energy.

A similar atomistic picture can be adapted to our evidences in the LTR regime, for $\varepsilon>500$ eV. In fact, STM topographies on the damage produced by single ion impacts on Ag(001) (Ref. 7) and on Pt(111) erosion[18] illustrate that the vacancy clusters produced from single ion collisions are surrounded by several clusters formed by the displaced adatoms, scattered on an area of average width of several nanometers. Within the crater width every correlation is supposed to be completely erased because of the hyperthermal collision transient. We propose to relate the ascending character of the wavelength, observed in our data, to the increase of the crater radius as a function of the energy which theoretically results from the molecular dynamics simulation of Ref. 19. From this viewpoint, the emergence of the LTR state for $\varepsilon>500$ eV can be interpreted as the onset of the formation of impact-induced "hot spots" which involve a local surface melting in the volume centered around the collision point.[17,18,20] This assumption is further corroborated by the slope relaxation at a higher impact energy reported in Fig. 4, since wider areas are affected by the thermal spike.[20] The loss of correlation for a higher energy can be reasonably associated either with the stronger excitation transferred to the surface atoms from the impinging ions or with an increase of the lateral extension of the impact crater.

On the other hand, we stress here the very difference of the decreasing law followed by the correlation length Λ within the RP state, when ε ranges from 200 eV up to 500 eV. Basing once again on an atomistic approach, this behavior can be interpreted in terms of the damage produced by the ion impact. Contrary to the presumed "thermal spike" regime, occurring for $\varepsilon>500$ eV, here we propose that the effect of the lower impact energy influences the variation of the defect production in the topmost surface layer. This conclusion is supported by the observation of a monotonic increase of the adatom yield with the energy on the Pt(111) surface in the energy range 0.04–10 keV, as follows from the STM analysis of single ion impacts[18] and from molecular dynamics simulations.[19] In other words, the relatively low energy of the impinging ions is here assumed to forbid ion implantation deep below the surface and the consequent collision cascade (which yields the local melting); the ions can be eventually reflected from the surface thus leaving adatom-vacancy pairs as resulting defects. This suggests to us to regard the role of the primary energy in analogy to the deposition flux in a growth experiment: an increment of the energy involves a larger concentration of mobile defects, essentially diffusing adatoms and less mobile vacancies, which after ion impact their rearrange to form stable nuclei. The decrease of the correlation length with increasing energy is thus a consequence of the increasing density of stable nuclei on the surface. We stress here that the *production* of adatoms during the collision transient is not very sensitive to the substrate crystallographic orientation and/or isotropy, which on the other hand affects the thermally activated diffusive relaxation of the adatoms.

It is interesting to elucidate how theoretical models based on a continuum approach can account for the change in the trend observed for the energy dependence of the correlation length and slope around the morphological transition point $\varepsilon^*=500$ eV. A general overview on the mostly adopted linear models pertaining to the evolution of the sputtered surfaces can give physical meaning to the observed trends depending on whether the usual thermal diffusion (TD) or an effective ion-induced surface diffusion (ISD) dominates surface restructuring.[21] Basing on the linear theory of surface erosion due to Bradley and Harper (BH),[22] Makeev *et al.* demonstrated that both contributions, the TD and ISD, are affected by a similar analytical curvature dependence, proportional to $\nabla^4 h$ when inserted in the continuum equation for the evolution of the surface height, even if they originate from intrinsically different processes which, in turn, present different dependences on the impact energy.[21] The case of a prevailing TD contribution can be fully treated basing on the original BH description, which predicts a relationship between Λ and ε of the form $\Lambda\propto\varepsilon^{-1/2}$, in qualitative agreement with the data referring to the RP regime (low energy range).[22] In this context an increase of ε results in an increase of the defect density surrounding the local impact site and thus in a higher nucleation density (decreasing Λ). We stress here that, to our knowledge, this is the first time a Bradley-Harper–like decreasing trend of Λ with increasing ε is observed: although the BH model is derived for a substrate for which the relaxation proceeds by isotropic surface diffusion, we believe that similar results are observed for the anisotropic case of

Cu(110) because the energy dependence of the wavelength at a fixed temperature (i.e., at a fixed diffusion rate either isotropic or anisotropic) is determined by the production of the adatoms during the hyperthermal transient following ion impact, which is relatively insensitive to the details of the crystallographic structure.

The subsequent increase of the $\Lambda(\varepsilon)$ function, above the transition point $\varepsilon^*=500$ eV, can be related to an enhanced efficiency of the ion-induced diffusive term which is known to determine a power law dependence $\Lambda \propto \varepsilon^{2m}$ where $m \leqslant \frac{1}{2}$ for energy $\varepsilon \leqslant 10$ keV.[21] From our experimental evidences the activation of the ISD term should result from an increase of the energy which additionally corresponds to the morphological transition into the LTR state. According to the atomistic viewpoint, this process operates whenever hot spots are formed as a consequence of the interaction with more energetic ions.

III. DYNAMICS OF THE RHOMBOIDAL PYRAMID STATE

Surface destabilization, giving rise to pattern formation, occurs even in the early stages of ion erosion due to the asymmetry of the incorporation rate into the ascending steps for the mobile species (in principle, adatoms and vacancies), and is often accompanied by a coarsening of the surface structures which, according to the phenomenological continuum theory,[8,23] can be described by a scaling behavior of the correlation length with a power law form: $\Lambda \sim t^n$. The dynamic exponent n for rippled patterns usually ranges from $\frac{1}{4}$ up to $\frac{1}{3}$ depending on the typology of the induced structures and, hence, on the kinetic constraints during ion irradiation (the erosion velocity, the diffusion rate limited processes, and the relaxation time of the mobile defects, for instance). However recent investigations on the real time evolution of rippled features on the ion-irradiated Cu(110) substrate by means of a grazing incidence x-ray scattering show that the dynamic exponent can vary from 0.08 to 0.1 depending on the substrate temperature during sputtering.[13] A very slow coarsening is as well recognized in the case of a glancing bombardment of the Cu(001) in ($n=0.06$).[24] Overall, while the wavelength increases with a slow rate, the surface roughness is conversely observed to follow a faster dynamics thus claiming for a leading role of the Ehrlich-Schwoebel effect in determining interlayer mass transport during ripple formation.

With the aim of extending these observations also to the RP regime, here we focus on the surface evolution on the ion-eroded Cu(110) surface under a decrease of the primary ion energy down to 400 eV, where, as discussed in the previous section, adatoms are supposed to be the main diffusing species. The experiments consist in several Xe^+ ion irradiations at different fluences, i.e., different sputtering time at the fixed flux $f=0.33$ ML/min, in the following condition: $T=230$ K and $\varepsilon=400$ eV. The surface morphology corresponding to each fluence is then monitored by means of SPA-LEED. A set of out-of-phase spot profiles ($S_z=1.88$) is reported in Fig. 5, in which the development of the RP pattern is observed from the early stages of the irradiation (few

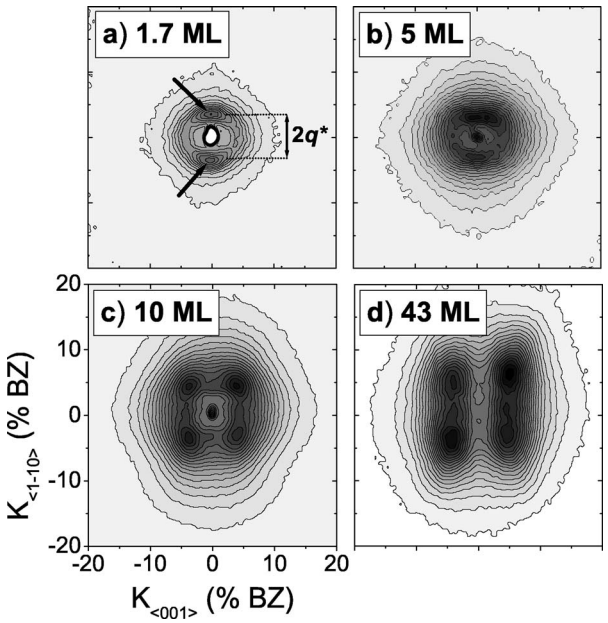

FIG. 5. Evolution of the out-of-phase spot profile ($S_z=1.88$) related to the ion irradiation at a different fluence, i.e., different sputtering time, in the fixed conditions: $T=230$ K; $\varepsilon=400$ eV; $f=0.33$ ML/min. The zone of a higher intensity along $\langle 1\bar{1}0\rangle$ inside the Henzler ring are pointed out by the arrows in panel (a). The radius q^* of the Henzler ring which informs on the mound-mound correlation is also indicated in panel (a).

ML of Xe^+ ions) up to high coverage of several tens of layers. Panel (a) is concerned with the irradiation of less than 2 equivalent ML after which the spot profile presents a peculiar ring around the (0,0) central peak and the high intensity of the central peak (saturated in the figure) indicates that (110) terraces still cover large areas of the surface. The sequence of one-dimensional (1D) linescans through the $\langle 1\bar{1}0\rangle$ reciprocal direction in Fig. 6 demonstrates that the radius q^* of the ring is not affected by change of the scattering phase, indicating that the features of the diffraction profile are not

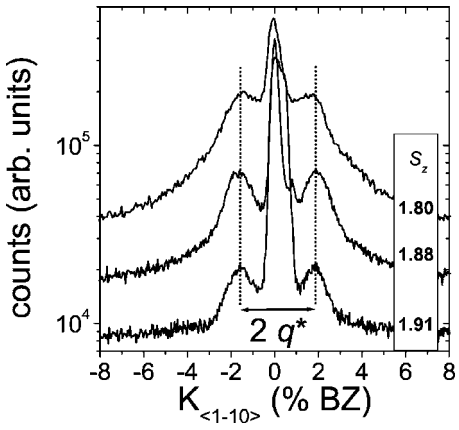

FIG. 6. Sequence of SPA-LEED linescans through the $\langle 1\bar{1}0\rangle$ reciprocal direction at different scattering phases S_z. Note the constant satellite separation, indicative of a distribution of laterally correlated mounds on the surface.

related to the formation of facets, but reflect the presence of the lateral correlation of the surface mounds with a characteristic separation $\Lambda^* \approx 142$ Å, given by the relation $\Lambda^* = 2\pi/q^*$. This is similar to the isotropic mound-mound lateral correlation occurring in the early stages of the Ag(001) homoepitaxy, a circular domain of higher intensity on the diffraction spot profile around the central Bragg peak, i.e., the so-called Henzler ring.[26] The Henzler ring exposed in Fig. 5(a) exhibits zones of higher intensity along the $\langle 1\bar{1}0\rangle_{\mathrm{rec}}$ direction (darker in the contour plot-short arrows) which correspond to a higher degree of lateral correlation in the $\langle 1\bar{1}0\rangle$ surface direction. After 5 ML irradiation [Fig. 5(b)] the Henzler ring can be still observed whereas the central peak intensity decreases sharply. Moreover the spot assumes a rhomboidal profile, most likely indicating the still imperfect rhomboidal shape of the mounds. The morphological arrangements resulting from an irradiation fluence below 5 ML consist in a distribution of nonfaceted mounds endowed with a more pronounced periodicity along the $\langle 1\bar{1}0\rangle$ surface direction. This configuration can be tentatively described with the following picture: the substrate temperature $T=230$ K at which the RP pattern is formed appears to be low enough to allow preferential diffusion of the mobile adatoms along the $\langle 1\bar{1}0\rangle$ channels; in the proximity of a step-edge oriented perpendicularly to the $\langle 1\bar{1}0\rangle$, the adatoms feel the additional Ehrlich-Schwoebel barrier and are preferentially reflected back towards the ascending steps traversing a characteristic temperature dependent diffusion length,[6] and coalesce into laterally correlated mounds.

The crossover towards a well-established RP morphology is achieved at 10 ML [Fig. 5(c)], where the fourfold symmetry of the out-of-phase spot profile along diagonal directions identifies the presence of the rhomboidal faceting. Contrary to the previous observations, now the diffraction peak is dominated by diffraction from the facets of the pyramids whose slope $\alpha_{\mathrm{RP}}{}^{10\ \mathrm{ML}}$ amounts to about 13.7° as determined by the observation of the satellite splitting increase when one moves away from the in-phase scattering condition. Increasing the sputtering time [at $\Psi=43$ ML in Fig. 5(d)] leads to the suppression of the central peak, due to the incremented roughness, and preserves the RP morphology with a fourfold splitting along diagonal directions. In this condition, the mounds become structurally steeper than in Fig. 5(c) as one can infer from the larger satellite separation at the same scattering phase ($\alpha_{\mathrm{RP}}{}^{43\ \mathrm{ML}} \approx 16.1°$).

The temporal sequence of Fig. 5 offers the first insight on the evolution of the surface morphology under the irradiation at the ion energy $\varepsilon=400$ eV. Recovering the structural properties of the surface pattern from the spot profiles allows us to access the details of the interfacial dynamics which can be directly compared to the scaling behavior theoretically obtained in the continuum approach of Refs. 8 and 9. The behavior of the correlation length Λ and the interfacial width W as a function of the sputtering time is illustrated in the diagrams of Fig. 7. In detail, Λ is obtained as usual from the shoulder of the anisotropic Henzler ring (below 5 ML irradiation) or from the constant satellite splitting near to the in-phase scattering condition (for higher irradiation coverage). On the other hand, W has been estimated from the width of the Gaussian fit to the experimental $G_0(S_z)$ function, for each single fluence. Only linescans through the directions in which satellites appear have been considered for deriving the $G_0(S_z)$ function. In Fig. 7(a) the correlation length Λ of the rhomboidal pyramids (filled diamonds) formed at $\varepsilon=400$ eV presents a power law dependence ($\Lambda \sim t^n$) with a dynamic exponent $n \approx 0.09$, which deviates from the faster coarsening predicted by the continuum approach of Refs. 8 and 9 and of the mostly used nonlinear models, essentially based on the Kardar-Parisi-Zhang ($n_{\mathrm{KPZ}} \approx 0.25$) or the Kuramoto-Shivashinsky ($n_{\mathrm{KS}} \approx 0.22-0.25$) equation.[21] However a similar behavior is as well reproduced by the scaling law of the LTR pattern obtained after Xe^+ ion irradiation at $\varepsilon=1000$ eV and reported, as a comparison, in Fig. 7(a) (open triangle). The scaling behavior of the LTR wavelength has a dynamic exponent $n \approx 0.084$ which was independently confirmed by a real-time x-ray diffraction study of Cu(110) erosion under similar sputtering conditions.[12] These results suggest that the RP and the LTR states are affected by very similar, comparatively slow, coarsening of the surface structures. In other words the time scaling of the lateral ordering is not affected by a change of the impact energy under ion-irradiation conditions.

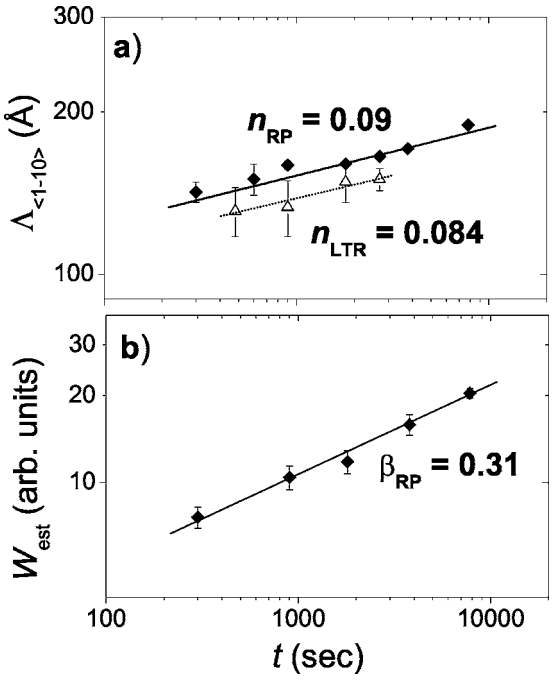

FIG. 7. Evolution of the correlation length $\Lambda_{\langle 1\bar{1}0\rangle}$ through the $\langle 1\bar{1}0\rangle$ (a) and of the estimated surface roughness W (b) for the surface patterns observed in Fig. 5 at different fluences. In panel (a) the scaling behavior of the LTR wavelength is also reported.

On the other hand, the rms roughness W obeys a steeper power law behavior ($W \sim t^{\beta}$) with a growth exponent $\beta \approx 0.31$, which agrees with the predictions of the continuum model in Ref. 8. The model predicts different scaling behaviors for the different morphological states of the phase diagram. In particular, away from transitions to the rippled states, a growth exponent $\beta_{\mathrm{RP}} \approx \frac{1}{4}$ is predicted for the pure

RP phase, while the growth exponent increases from the latter value whenever the system approaches the condition in which all zeros $\mathbf{m}^*$ of the nonequilibrium $\mathbf{J}_{\mathbf{up}}$ current are unstable (this phase is denoted as "buckled ripples" in Ref. 8). A faster coarsening, with $\beta_{\mathrm{RP}} \approx 0.32$, which is consistent with our experimental result, is then found in the RP region close to the buckled rippled state.

IV. UNSTABLE CHARACTER OF THE RP STATE

The structural characterization exposed in Ref. 1 emphasizes how the step arrangement of the RP's strays from the energetically favored orientation of the step edges in a fcc (110) terminated surface, which corresponds to the close-packed $\langle 1\bar{1}0\rangle$ channels. In spite of the low symmetry orientations of the RP contour steps, the main diffusive processes, i.e., the processes endowed with a comparatively lower activation energy, take place essentially via *intralayer* surface diffusion, governed by the two nonequivalent energetic barriers $E^D_{\langle 1\bar{1}0\rangle}$ and $E^D_{\langle 001\rangle}$, and *interlayer* massive transport biased uphill by the extra ES barriers $E^S_{\langle 1\bar{1}0\rangle}$ and $E^S_{\langle 001\rangle}$ at the step edges.[30] Therefore, a very delicate compromise between the hierarchy of the activated diffusive processes and the nature of the diffusing species should establish in the RP regime in order to let the thermodynamically unstable step edges of the RP islands form. If we now also take into account the proximity in the morphological phase diagram of the observed RP pattern to the unstable buckled rippled state (as discussed in the previous section), the resulting scenario suggests a strongly unstable character of the RP features, meaning that the regular step fronts of the RP facets undergo a fast thermal relaxation upon annealing. Aiming to check the unstable nature of the RP pattern upon thermal perturbation, we perform an annealing experiment on the RP pattern obtained after irradiating 21 ML at $T=230$ K and $\varepsilon=400$ eV, by monitoring in real time the out-of-phase spot profile at the constant temperature $T_{\mathrm{A}}=245$ K, i.e., slightly above the formation temperature of the RP state such as that reported in Fig. 2. Three representative snapshots recorded at different times during the annealing experiment are reported in Fig. 8. Figure 8(a) shows the initial RP state as observed immediately after ion irradiation. After 8 min of annealing the fourfold satellite on the diffraction map, peculiar of the RP faceting, has completely decayed and a one-dimensional lateral correlation becomes observable as results from the twofold symmetry of the out-of-phase spot profile of Fig. 8(b). Here the satellites due to the lateral correlation along the $\langle 1\bar{1}0\rangle$ becomes evident since the satellites due to facets have decayed. This fact is further corroborated by noting that an identical satellite separation is observed in Fig. 8(d) for the near-in-phase linescan taken before the annealing (open circles) and the out-of-phase linescan after 8 min long annealing (full circles). The characteristic satellites of the one-dimensional lateral correlation are almost completely vanishing after 118 min of annealing, whereas the increase of the central Bragg peak intensity indicates that larger portions of the surface have become flat [see Fig. 8(c)].

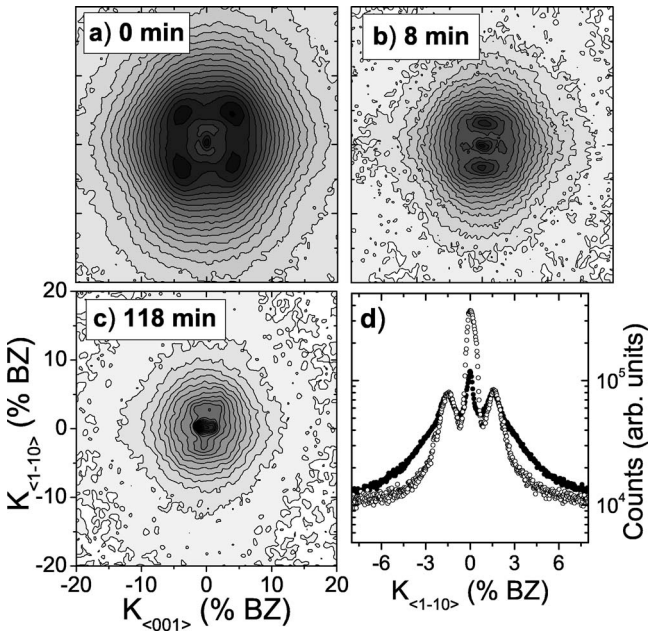

FIG. 8. An annealing experiment at $T=245$ K. Out-of-phase spot profiles ($S_z=1.88$) registered at different times during the annealing: (a) prior to the annealing treatment; (b) after 8 min long annealing; (c) after 118 min long annealing. (d) Comparison between a near-in-phase linescan ($S_z=1.92$) prior to the annealing procedure (open circles) and an out-of-phase linescan after 8 min of annealing at $T=245$ K (full circles). Note the equivalent satellite separation on both linescans.

In order to get additional details on the vertical relaxation of the RP pattern, the experimental G_0 function, calculated at the fixed phase $S_z=1.88$, is plotted as function of the annealing time in Fig. 9. The G_0 values follow a power law increase ($G_0 \sim t^a$), with exponent $a=0.7$, indicating the smoothing of the surface profile. After about 51 min long annealing at $T_{\mathrm{A}}=245$ K, G_0 appears to grow at a slower rate indicating that the surface roughness decay proceeds more slowly, probably because bass transport proceeds over more extended terraces. Overall, G_0 is observed to grow at a rate of about 0.3 arbitrary units in 51 min, which quantitatively corresponds to a reduction of the surface roughness of about

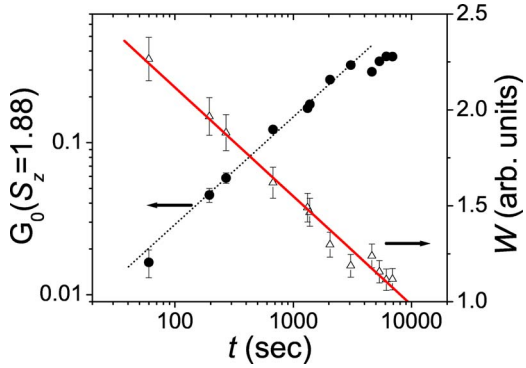

FIG. 9. (Color online) Plot of the experimental G_0 function, calculated at the phase $S_z=1.88$, vs annealing time. The line identifies a power law fit to the data, giving the exponent $a \approx 0.7$.

55% with respect to the quantity revealed prior to the annealing (at $t=0$ sec). In more detail, the surface roughness W has been estimated from the dependence of G_0 on the scattering phase, and plotted in Fig. 9 as a function of the annealing time (open triangles), proving that the relaxation dynamics of the surface profile follows an exponential decay. The latter behavior claims for an adatom attachment-detachment limited kinetics during the surface equilibration at the given temperature $T_A=245$ K,[29] which is known to be governed by step traversal processes of the adatoms emitted from the steps. The importance of step traversal processes during the relaxation of the surface profile should be enhanced by the presence of narrow terraces bounding the RP facets at the early stages of annealing.

V. DISCUSSION AND CONCLUSIONS

After documenting in Sec. I the formation of the RP pattern experimentally observed for the first time in Ref. 1, in Sec. II we have shown how the decrease of the impact energy, mandatory to observe the RP state (see Fig. 2), corresponds to a reduction of the adatom concentration during Xe^+ ion bombardment, which is consistent with the experimental findings of Michely and Teichert[18] and the theoretical results of Ghaly and Averback,[20] both on Pt(111) erosion. In Ref. 1 we also argued that the role of the impact energy in terms of pattern formation can be mimicked by acting both on the ion flux or on the substrate temperature, the former being related to the relaxation time for a mobile defect between subsequent collisions and the latter to the rate of a diffusive event. The two key quantities governing pattern formation under the regime of low energy ion irradiation, i.e., when the ion impact procures damages limited to the top surface layers, are the concentration and the diffusivity of the displaced adatoms. While the substrate temperature determines the adatom diffusivity via Arrhenius-like kinetic processes, the adatom concentration can be controlled by varying the ion flux as well as the impact energy.

To provide more solid evidence of the latter effect, from Ref. 1 we resume in Figs. 10(a)–10(c) the set of spot profiles at increasing fluxes which qualitatively reproduces a similar sequence to that shown in Fig. 2 as a function of the energy. The panels show that, starting from the usual RP configuration obtained at $f=0.33$ ML/min, $\varepsilon=400$ eV and $T=230$ K [Fig. 10(b)], an increase of the flux up to $f=3$ ML/min and a decrease of the flux down to $f=0.1$ ML/min involves the formation of a LTR [Fig. 10(a)] and a HTR pattern [Fig. 10(c)], respectively. Limiting the interest to the range of flux in which the RP state forms (approximately from 0.3 ML/min up to 2 ML/min), the flux dependence of the correlation length, plotted in Fig. 10(d) (square points), presents a decreasing behavior such as the one observed in the RP regime of Fig. 4, when the independent variable was the energy. From direct comparison, the data related to the RP correlation length as a function of the energy are also reported on the diagram of Fig. 10(d) (circle points). The similar descending trends illustrated in the diagram of Fig. 10(d) corroborate the idea that, in proper ranges, variations of flux are roughly equivalent to variations of the energy in terms of the induced surface morphologies.

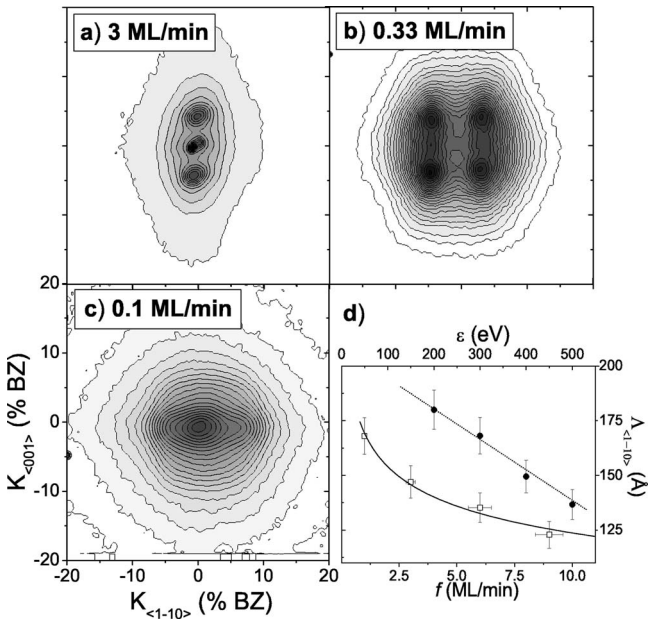

FIG. 10. Out-of-phase spot profiles ($S_z=1.88$) after ion irradiation of Cu(110) at the energy $\varepsilon=400$ eV, the temperature $T=230$ K, and the fluence $\Psi=21$ ML, using the flux f as a parameter: (a) $f=3$ ML/min; (b) $f=0.33$ ML/min; (c) $f=0.1$ ML/min. (d) Flux dependence of the correlation length Λ of the RP pattern observed within the range 0.3 ML/min$\leqslant\varepsilon\leqslant$2 ML/min (open square) compared to the energy dependence of the Λ obtained in the range 300 eV$\leqslant\varepsilon\leqslant$500 eV (full circles). The two lines in panel (d) are guides to the eye.

The effects of energy variations on the surface damaging can be indeed displayed by considering the following arguments. The number of adatoms created during the erosion for $\varepsilon\leqslant 500$ eV exceeds that of sputtered atoms since the creation of an adatom needs less collisional energy than that needed for creating a sputtered adatom.[18] As a consequence the surface morphology is characterized by the presence of both adatoms and vacancies, eventually aggregated in clusters, but the former species are prevailingly mobile, due to their higher diffusivity at $T=230$ K.[28] Some important consequences follow from the previous considerations: (a) the adatoms (and their clusters) are the "dominant subjects" of the kinetic surface processing within the RP regime; (b) the adatom yield is low enough to afford a larger relaxation of the mobile adatoms (compared to the LTR case with $\varepsilon>600$ eV), before being sputtered away or incorporated in other surface structures, such as islands, steps, or kinks. Statements (a) and (b) still hold for a variation of the ion flux as well as for a variation of the impact energy since both govern the concentration of adatoms (and vacancies) at a given temperature. Especially during the erosion at 200 eV the adatom concentration is further reduced and the system tends to mimic the homoepitaxial condition evolving into the HTR state. In the extreme case of a pure homoepitaxial growth, where by definition the adatoms are the only diffusing defects, the self-organization of the HTR state, in the similar Ag(110) surface, is indeed observed to occur with a thermal shift towards lower substrate temperatures compared to the sputtering analog.[6] The temperature shift between

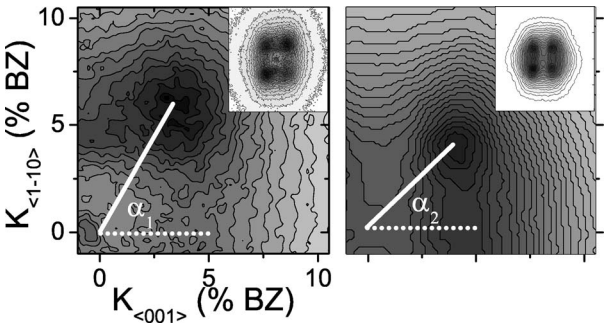

FIG. 11. Magnifications on a satellite peak in the out-of-phase spot profiles of RP patterns obtained at the same fluence $\Psi=21$ ML for the two different fluxes: (left) $f=1$ ML/min; (right) $f=0.33$ ML/min. The other sputtering parameters are set as in Fig. 10.

crystal growth and erosion experiments is explained by the different activation threshold for the diffusion of the respective mobile defects, which in the former case exclusively consist in single adatoms and in the latter case mostly correspond to slowly diffusing clusters of adatoms, at least until the mobility of vacancy clusters is hindered.[7] We also underline here that, once established, the nature of the mobile species, a primary role in pattern formation is played by the strongly anisotropic diffusion rates descending from the rectangular symmetry of the (110) class of surfaces.

The interplay of the adatom concentration and diffusivity allows us to unbalance the directionality of the $\mathbf{J_{up}}$ current. The capability to tune the $\mathbf{J_{up}}$ orientation can be experimentally checked in more details by investigating the effect of slight variations of the flux on the RP structure. In fact, a deeper insight on the flux dependence of the RP state reveals that the step arrangement (and orientation) of a rhomboidal pyramid, i.e., the RP structure as deduced from the diffraction profile in Fig. 2(d), is not unique, but undergoes a structural modification under variations of the ion flux. The nonuniqueness of the RP state is demonstrated by the pair of spot profiles in Fig. 11 which refer to RP patterns obtained after the same fluence $\psi=21$ ML at two different fluxes: 1 and 0.33 ML/min, respectively. Panel (a) reproduces a magnification around a satellite of the same RP spot profile as observed in Fig. 2(d) (rectangular shaped spot profile). Here the kinked step edges run along $\langle 1\bar{1}2\rangle$ surface directions forming an angle of about $\alpha_1=35°$ with the $\langle 001\rangle$ high symmetry axis as deduced in Fig. 11(a) from the position of the satellite compared to the (0,0) peak point. On the other hand, Fig. 11(b) presents a different, squared shape spot profile [compare the insets of panels (a) and (b)] in which, according to the same reasoning as above, the angle of the majority steps is $\alpha_2\approx 45°$ with respect to the $\langle 001\rangle$ directions. This reflects the presence of kinked step edges along the $\langle 3\bar{3}2\rangle$ directions). We denote the two RP motifs with $RP_>$ [Fig. 11(a)] and $RP_<$ [Fig. 11(b)] to recall that they derive from the use of two comparatively different fluxes. We stress here that the different orientation of majority steps in the two cases involves a real-space shape of the mounds, which corresponds to a rhomboidal layout squashed in the $\langle 1\bar{1}0\rangle$ for the $Rp_>$ fashion [in Fig. 11(a)] and to a squared structure with diagonals along the high symmetry surface directions, $\langle 1\bar{1}0\rangle$ and $\langle 001\rangle$, for the $RP_<$ fashion [in Fig. 11(b)]. If we insert the two different RP motifs inside the framework of the consecutive transitions observed in Fig. 2, we realize that the $RP_>$ fashion approaches more the $\langle 001\rangle$ elongated LTR corrugations, whereas the $RP_<$ distortion from the squashed rhomboidal shape suggests a progressive transformation into a HTR-like structure. This scenario can be rationalized in terms of the following picture. The leading adatom currents $\mathbf{J}_{\langle 1\bar{1}0\rangle}(\mathbf{m})=[(\pm J_1(\mathbf{m}),0)$ and $\mathbf{J}_{\langle \mathbf{001}\rangle}(\mathbf{m})=(0,\pm J_2(\mathbf{m}))]$, flowing along the main surface directions (denoted in the brackets by the indexes 1 and 2), mutually interact, then inducing an effective current density $\mathbf{J}^*=(J_1,J_2)=\mathbf{J}_{\rm up}(\mathbf{m}^*)$ which determines the RP morphology. Artificial modifications of the $\mathbf{J}_{\langle 1\bar{1}0\rangle}$ and $\mathbf{J}_{\langle 001\rangle}$ currents can be achieved by acting on the impact energy, the ion flux, or the substrate temperature and result in a change of the effective orientation of the $\mathbf{J}^*$ current which, in turn, give rises to the consecutive transitions between morphological states, including the two RP motifs. This qualitative picture should elucidate the vectorial character of the current density described in Refs. 8 and 9 as a function of the dimensionless parameters used in the continuum model of Ref. 8. The same arguments should be applicable also to a carefully tailored growth experiment though the proper conditions for inducing the RP morphology are restricted to a very narrow range of the substrate temperatures and/or the deposition fluxes. Note that the transition between RP, LTR, and HTR morphologies takes place with changes of the substrate temperature which amount to few tens of **K**.

We also argue that the instability provoking the formation of the RP state is governed by the vectorial adatom current $\mathbf{J}_{\rm up}$ essentially due to the nonequivalent Ehrlich-Schwoebel barriers at the step edges along the two main surface directions $\langle 1\bar{1}0\rangle$ and $\langle 001\rangle$. The existence of two nonequivalent diffusion currents along the symmetry directions was already considered by Rusponi *et al.*[25] in order to explain the formation of the sputter induced rippled states in terms of effective erosive terms (with a curvature dependence proportional to the second order derivatives $\partial_x^2 h$ and $\partial_y^2 h$ inside the Bradley-Harper equation[22]) which account for the anisotropic ES extra-barrier $E^S_{\langle 1\bar{1}0\rangle}=0.19$ eV and $E^S_{\langle 001\rangle}=0.27$ eV,[27,29] however, in that case the two currents were treated independently. In (001) terminated surfaces, this mechanism gives rise to a mound formation characterized by a growth rate with $n=\frac{1}{4}$,[10,11,14] which considerably differs from the slow coarsening observed here for the RP and the LTR pattern. Our present measurements extend the argument of Rusponi *et al.*[25] suggesting that a vectorial sum of nonequivalent $\mathbf{J}_{\rm up}$ components along the main surface direction is directly responsible for the selection of out-of-equilibrium facet such as the RP ones. From this point of view, the RP domain occurs from the balance of these components, in an intermediate position between the rippled states. However, the resulting scaling laws of the correlation length and of the surface roughness of the patterns present a slower coarsening

compared to growth experiments in systems with an efficient ES barrier at the step edge. In fact, when the surface evolution is studied under ion sputtering at $\varepsilon=400$ eV, a comparatively low dynamic coefficient $n\approx 0.1$ is found which is compatible with the scaling behavior of the LTR regime obtained at ion energies $\varepsilon \geqslant 600$ eV. The slow dynamics can rely on a slight distortion from a Bradley-Harper–like evolution of the sputtered surface as suggested by Chan *et al.*[24] However, this viewpoint suffers from the some shortcomings. Firstly, contrary to the exponential increase predicted by the Bradley-Harper model, the growth rate of the interfacial width and, hence, of the ripple amplitude is here observed to follow a power law dependence. Secondly, the energy dependence of the correlation length between the surface structures indicates the activation of an ion-induced surface diffusion term in the LTR regime. On the other hand, the qualitative analogy between our experimental evidences and the theoretical predictions of Refs. 8 and 9 support the description in terms of the phenomenological continuum theory applied to the case of fcc(110) terminated surfaces in terms of net defect currents, which disregards the atomistic details of the ion-induced damaging, but concentrates on the thermally activated relaxation of defects produced when the surface is destabilized by the ion collisions.[8,9]

In conclusion, after a detailed overview of the phenomenology of the RP morphological state formation observed for the first time in Ref. 1, we explore the dynamics of the relevant surface processes active under ion erosion at a low energy by studying the evolution of the RP state. This allows us to compare the time scaling of the features qualifying the time evolution of the surface profile, with the theoretical predictions of Ref. 8. We elucidate the unstable nature of the RP features by observing the rapid decay of the RP facets after annealing slightly above their formation temperature. Finally, we demonstrate that in the low energy range ($\varepsilon \leqslant 500$ eV) where the RP morphological state is formed, the lateral correlation length of the nanostructures and their facet slope scale in a manner which is qualitatively similar to a deposition experiment.

*Present address: CNR-INFM MDM National Lab, via C. Olivetti 2, I-20041 Agrate Brianza (Milano). Email address: alessandro.molle@mdm.infm.it

†Corresponding author. Email address: buatier@fisica.unige.it

[1] A. Molle, F. Buatier de Mongeot, A. Molinari, F. Xiaerding, C. Boragno, and U. Valbusa, Phys. Rev. Lett. **93**, 256103 (2004).

[2] S. Rusponi, G. Costantini, F. Buatier de Mongeot, C. Boragno, and U. Valbusa, Appl. Phys. Lett. **75**, 3318 (1999).

[3] S. Rusponi, C. Boragno, and U. Valbusa, Phys. Rev. Lett. **78**, 2795 (1997).

[4] M. V. Ramana Murty, T. Curcic, A. Judy, B. H. Cooper, A. R. Woll, J. D. Brock, S. Kycia, and R. L. Headrick, Phys. Rev. Lett. **80**, 4713 (1998).

[5] U. Valbusa, C. Boragno, and F. Buatier Mongeot, J. Phys.: Condens. Matter **14**, 8153 (2002).

[6] F. Buatier de Mongeot, G. Costantini, C. Boragno, and U. Valbusa, Phys. Rev. Lett. **84**, 2445 (2000).

[7] G. Costantini, F. Buatier de Mongeot, C. Boragno, and U. Valbusa, Phys. Rev. Lett. **86**, 838 (2000).

[8] L. Golubovic, A. Levandovsky, and D. Moldovan, Phys. Rev. Lett. **89**, 266104 (2002).

[9] A. Levandovsky, L. Golubovic, and D. Moldovan (unpublished).

[10] M. Siegert and M. Plischke, Phys. Rev. Lett. **73**, 1517 (1994).

[11] J. Villain, J. Phys. (Paris) **1**, 19 (1991).

[12] C. Boragno, F. Buatier de Mongeot, G. Costantini, A. Molle, D. deSanctis, U. Valbusa, R. Felici, and S. Ferrer, Phys. Rev. B **68**, 094102 (2003).

[13] A.-L. Barabási and H. E. Stanley, *Fractal Concepts in Surface Growth* (Cambridge University Press, Caambridge, 1994).

[14] J. Krug, Adv. Phys. **46**, 139 (1997).

[15] J. Wollschlager, E. Z. Luo, and M. Henzler, Phys. Rev. B **57**, 15541 (1998).

[16] C. C. Umbach, R. L. Headrick, and K.-C. Chang, Phys. Rev. Lett. **87**, 246104 (2001); S. Habenicht, K. P. Lieb, J. Koch, and A. D. Wieck, Phys. Rev. B **65**, 115327 (2002); T. K. Chini, M. K. Sanyal, and S. R. Bhattacharyya, *ibid.* **66**, 153404 (2002).

[17] S. van Dijken, D. de Bruin, and B. Poelsema, Phys. Rev. Lett. **86**, 4608 (2000).

[18] Th. Michely and C. Teichert, Phys. Rev. B **50**, 11156 (1994).

[19] E. M. Bringa, K. Nordlund, and J. Keinonen, Phys. Rev. B **64**, 235426 (2001).

[20] M. Ghaly and R. S. Averback, Phys. Rev. Lett. **72**, 364 (1994).

[21] M. A. Makeev, R. Cuerno, and A.-L. Barabási, Nucl. Instrum. Methods Phys. Res. B **197**, 185 (2002).

[22] R. M. Bradley and J. M. E. Harper, J. Vac. Sci. Technol. A **6**, 2390 (1988).

[23] D. Moldovan and L. Golubovic, Phys. Rev. E **61**, 6190 (2000), M. Siegert, Phys. Rev. Lett. **81**, 5481 (2000).

[24] W. L. Chan, N. Pavenayotin, and E. Chason, Phys. Rev. B **69**, 245413(R) (2004).

[25] S. Rusponi, G. Costantini, C. Boragno, and U. Valbusa, Phys. Rev. Lett. **81**, 4184 (1998).

[26] L. Bardotti, C. R. Stoldt, C. J. Jenks, M. C. Bartelt, J. W. Evans, and P. A. Thiel, Phys. Rev. B **57**, 12544 (1998).

[27] F. Montalenti and R. Ferrando, Phys. Rev. B **59**, 5881 (1998); P. Stoltze, J. Phys.: Condens. Matter **6**, 9495 (1994)].

[28] R. Ferrando (private communication).

[29] N. Israeli and D. Kandel, Phys. Rev. B **62**, 13707 (2000); Phys. Rev. Lett. **88**, 169601 (2002).

[30] An adatom which attempts a step traversal perceives a global energetic barrier E^{SE} corresponding to the sum of the terrace diffusion activation energy E^D with the extra ES barrier E^S at the perpendicular step. For the Cu(110) surface: $E^D_{\langle 1\bar{1}0\rangle}=0.29$ eV, $E^S_{\langle 001\rangle}=0.27$ eV then $E^{ES}_{\langle 1\bar{1}0\rangle}=E^D_{\langle 1\bar{1}0\rangle}+E^S_{\langle 001\rangle}=0.56$ eV and $E^D_{\langle 001\rangle}=0.42$ eV, $E^S_{\langle 1\bar{1}0\rangle}=0.19$ eV then $E^{ES}_{\langle 001\rangle}=E^D_{\langle 001\rangle}+E^S_{\langle 1\bar{1}0\rangle}=0.61$ eV (Ref. 27).